Surg Endosc (2005) 19: 1652–1665
DOI: 10.1007/s00464-005-0159-9

SURGICAL ENDOSCOPY
and Other Interventional Techniques

Comparative anatomy of the porcine and human thoracic spines with reference to thoracoscopic surgical techniques

H. Bozkus,[1] N. R. Crawford,[2] R. H. Chamberlain,[2] T. D. Valenzuela,[2] A. Espinoza,[2] Z. Yüksel,[2] C. A. Dickman[2]

[1] Department of Neurosurgery, VKV American Hospital, Güzelbahçe Sk. No. 20, 80200, Nisantasi, Istanbul, Turkey
[2] Spinal Biomechanics Research Laboratory, Barrow Neurological Institute, 350 West Thomas Road, Phoenix, AZ 85013, USA

Received: 22 March 2005/Accepted: 26 May 2005/Online publication: 5 October 2005

Abstract
Background: This study compared porcine and human thoracic spine anatomies for a better understanding of how structures encountered during thoracoscopy differ between training with a porcine model and actual surgery in humans.
Methods: Parameters were measured including vertebral body height, width, and depth; disc height; rib spacing; spinal canal depth and width; and pedicle height and width.
Results: Although most porcine vertebral structures were smaller, porcine pedicle height was significantly greater than that of humans because the porcine pedicle houses a unique transverse foramen. The longus colli and psoas attach, respectively, to T5 and T13 in swine and to T3 and T12 in humans. In swine, the azygos vein generally was absent. The intercostal veins drained into the hemiazygos vein.
Conclusions: Several thoracoscopically relevant anatomic differences between human and porcine spinal anatomies were identified. A thoracoscopic approach in a porcine model probably is best performed from the right side. The best general working area is between T6 and T10.

Key words: Comparative anatomy — Porcine model — Thoracic spine — Thoracoscopy

Minimally invasive video-assisted thoracic spine surgery currently is used for a variety of surgical procedures such as sympathectomy, discectomy, corpectomy, spinal reconstruction, biopsy, and tumor resection [6, 9–11, 14, 18, 21]. These thoracoscopic surgical techniques often are taught to spine surgeons through hands-on training courses. The porcine model is excellent for such training because animals are readily available and inexpensive, allowing surgeons to practice in a living system before performing thoracoscopic techniques in a human patient [2, 3, 5, 8, 13, 15, 16, 19, 22]. In the porcine model, various surgical strategies can be simulated that are infeasible in a human cadaveric model, such as retracting the lung, maintaining a bloodless field during different techniques, coping with fogging of lenses, and dissecting living tissues in their physiologic conditions [7, 16]. The disadvantage with the porcine model is the dissimilar anatomies of the human and porcine thoracic spinal regions.

This study aimed to describe and quantify important anatomic structures of the porcine thoracic spine encountered during thoracoscopic spine surgical training. Differences between these structures and the corresponding structures in humans are qualitatively described and quantitatively compared with previously published data. Considerations are given that surgeons should understand in applying the knowledge gained during thoracoscopic training with swine to subsequent human patients.

Methods

Anatomic measurements and observations were obtained in swine from direct visualization, plain film radiography, microsurgery, and endoscopic exploration.

Specimen preparation

For most anatomic measurements, 10 cadaveric New Hampshire swine (5 males and 5 females; weight, ~30 kg; age, 6 months) were used. All the animals were available for our use after their termination from protocols approved by the animal care and use committee in our institution. After termination, specimens were kept in a cold room at 4°C for a maximum of 12 h before dissection.

After exposure of the thoracic spine, the ribs were transected 25 cm bilaterally from the midsagittal plane, and the spine segment from the caudalmost cervical to the rostralmost lumbar vertebra (identified by the absence of ribs) was isolated. This spine segment with vascular

Correspondence to: C. A. Dickman

structures intact was removed *en bloc*. Specimens were studied immediately after retrieval, and if further study time was needed, they were wrapped in saline-soaked gauze, frozen, and stored at −20°C.

At a later date, an additional 10 cadaveric whole swine (6 males and 4 females; weight, ~30 kg; age, 6 months) and 10 human cadaveric torsos (7 males and 3 females; mean age, 66 years; range, 57–81 years) were studied to determine intercostal spacing. An incision was made with a scalpel in the midaxillary coronal plane, and tissues were separated from the ribs for direct measurement of intercostal spacing with digital calipers (precision, ±0.1 mm; Mitutoyo Digimatic Calipers, Tokyo, Japan).

Microscopic procedure

The intercostal anatomy, bony structures, and articular surfaces of the thoracic spinal column were evaluated in four specimens using an operative microscope (MKM; Carl Zeiss, Oberkochen, Germany). All microdissections were performed on the day of specimen retrieval. Photographs and qualitative findings were recorded.

Radiographic measurements

Lateral plain film x-rays of each thoracic spine without ribs were taken at a 1-m focus-film distance. Anteroposterior x-rays of four specimens also were taken. The intervertebral disc height was measured from lateral images using digital calipers along the anterior margin, the midpoint, and the posterior margin of the vertebral body for each specimen. A metallic ruler was placed next to each specimen during the radiographic examinations, and measurements were adjusted to ensure that there were no magnification errors.

Anatomic measurements

After all measurements and observations of fresh specimens were completed, the specimens were boiled in a strong solution of household nonchlorine whitening laundry detergent (Tide with Bleach; Procter and Gamble, Cincinnati, OH, USA) for 1 to 3 h to facilitate the removal of soft tissues with minimal damage to the bony and cartilaginous structures.

After drying for at least 1 day, each vertebra was numbered, and the spinous process was clamped in a vise. The three-dimensional coordinates of 17 prechosen landmarks on each vertebra were identified and recorded using the Optotrak 3020 with a 6-marker digitizing probe (Northern Digital, Waterloo, Ontario, Canada; Fig. 1). For each vertebra, 14 parameters were calculated using these digitized points (Table 1).

Endoscopic procedure

After all data from quantitative measurements, radiographic examinations, and microsurgical inspection were recorded, one live animal was studied endoscopically under an approved teaching protocol to verify and elaborate upon findings.

Statistical analysis

All anatomic measurements are expressed as the mean ± standard deviation. Statistical differences were calculated using analysis of variance (ANOVA) followed by the Tukey test. Each of the linear parameters was compared with the results from a published study of human thoracic anatomy [17]. Statistical comparison with the results for human anatomy was performed using two-tailed nonpaired Student's *t*-tests. All p values less than 0.05 were considered significant.

Results

Regional divisions

All the porcine thoracic spines studied were composed of 15 or 16 vertebrae, whereas the human thoracic spine has 12 vertebrae. The thoracic vertebrae of the porcine specimens studied had three distinct regions of differing geometry (Fig. 2): upper thoracic (T1–T2), middle thoracic (T3–T10) and lower thoracic (T11–T15 or −16). We found the xiphoid process to be aligned with the sixth intercostal space and the T5–T6 disc in all the animals studied.

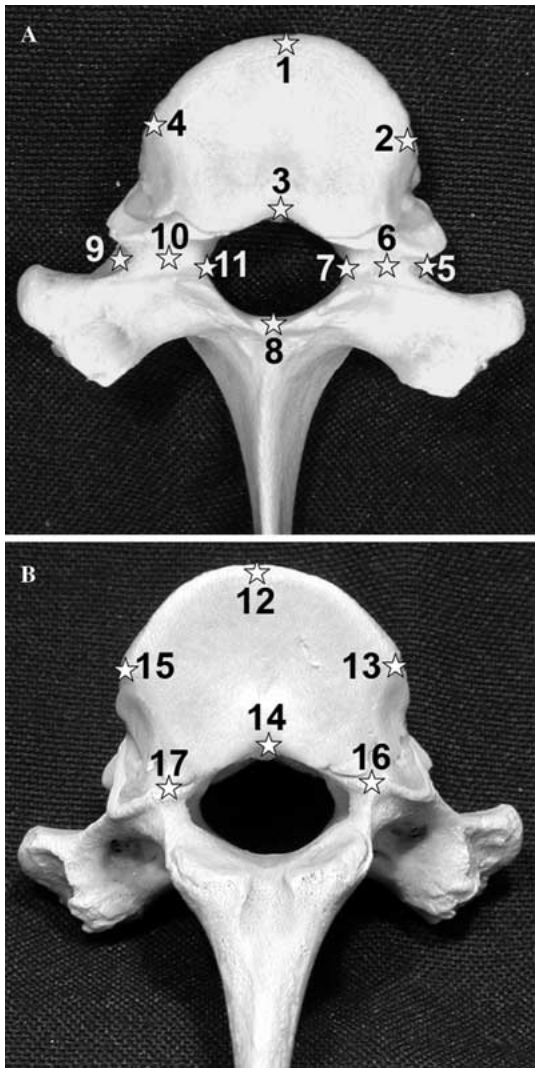

Fig. 1. Sequential order and sites of digitization of bony landmarks used in anatomic measurements of porcine vertebrae. **A** points on the rostral vertebral surface. **B** points on the caudal vertebral surface.

Selected chest cavity organs and muscles

Similar to their human counterparts, the porcine trachea and esophagus were located immediately ventral to the thoracic spine. The esophagus ran to the right of the aorta initially, and later ran anteriorly to it until it terminated at the diaphragm. The caudal end of the longus colli muscle was attached to the fifth thoracic vertebra. In the human, this muscle terminates at the third thoracic vertebra caudally. The rostral end of the psoas muscle terminated across the lateral body of the 13th

Table 1. Parameters obtained from bony landmarks

Abbreviation	Parameter (units)	Formula
AVBH	Anterior vertebral body height (mm)	P_1–P_{12}
PVBH	Posterior vertebral body height (mm)	P_3–P_{14}
UED	Upper end plate depth (mm)	P_1–P_3
UEW	Upper end plate width (mm)	P_4–P_2
UEA	Upper end plate area (mm^2)	$\pi\left(\frac{UED}{2}\right)\left(\frac{UEW}{2}\right)$
LED	Lower end plate depth (mm)	P_{12}–P_{14}
LEW	Lower end plate width (mm)	P_{15}–P_{13}
LEA	Lower end plate area (mm^2)	$\pi\left(\frac{LED}{2}\right)\left(\frac{LEW}{2}\right)$
SCD	Spinal canal depth (mm)	P_3–P_8 (transverse plane coordinates only)
SCW	Spinal canal width (mm)	P_{11}–P_7
RPW	Right pedicle width (mm)	P_7–P_5 (transverse plane coordinates only)
RPH	Right pedicle height (mm)	P_6–P_{17} (rostrocaudal coordinates only)
LPW	Left pedicle width (mm)	P_9–P_{11} (transverse plane coordinates only)
LPH	Left pedicle height (mm)	P_{10}–P_{16} (rostrocaudal coordinates only)

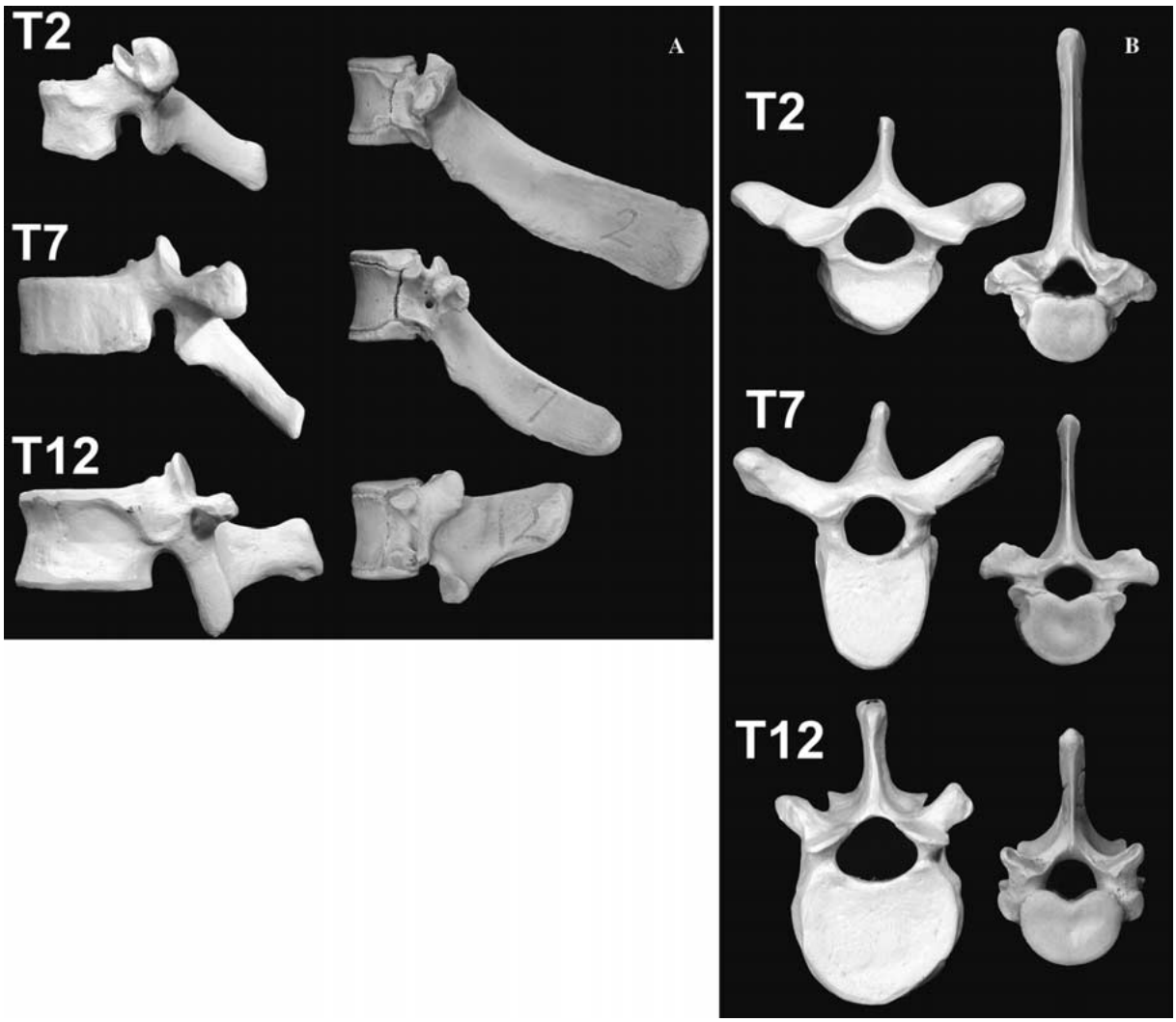

Fig. 2. Representative dried human and porcine vertebrae from the upper thoracic region (T2), the middle thoracic region (T7), and the lower thoracic region (T12). **A** lateral views. **B** axial views.

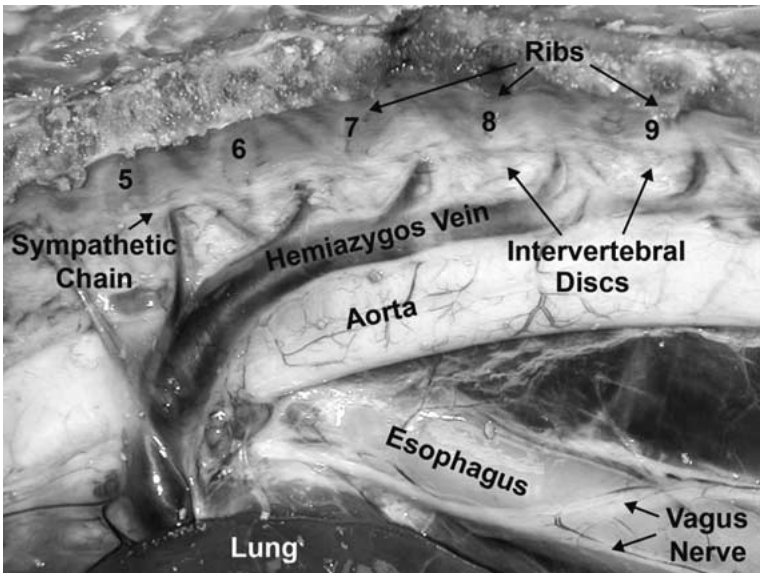

Fig. 3. Prominent structures in the left porcine thorax. The hemiazygos vein typically is present only on the left side and drains directly into the superior vena cava.

thoracic vertebra. In the human, the psoas terminates at the 12th thoracic vertebra.

Nerve anatomy

The right vagus nerve ran posteroinferiorly on the right surface of the trachea and adjacently to the esophagus (Fig. 3). The left vagus nerve ran laterally to the aorta. As in the human, the sympathetic chain overlaid the heads of the ribs and the segmental vessels immediately beneath the surface of the parietal pleura (Figs. 3 and 4). Although the sympathetic chain was easily visualized, the sympathetic ganglia and nerve of Kuntz were too small to be identified.

Venous structure

In the left thorax, the aortic arch was positioned laterally to the trachea and esophagus. The descending aorta ran ventrolaterally to the thoracic spine. On the right side, unlike the human, there usually was no visible azygos vein, although a rudimentary azygos vein was present in 2 of 11 animals studied. All intercostal veins (except the most superior veins) usually drained into the hemiazygos vein, which was located in the left thorax. The hemiazygos vein was positioned medially to the rib heads on the posterolateral side of the descending aorta (Fig. 3). It emptied directly into the superior vena cava. In the human, this vein drains into the azygos vein.

The drainage of the first four intercostal veins and the source of the first intercostal artery were not identified during thoracotomy. The intercostal arteries arose from the descending aorta (except for the most superior arteries) and ran parallel to the intercostal veins, across the middle of the vertebral bodies. The intercostal vein, artery, and nerve lay beneath the inferior edge of the rib as in the human.

Also encountered during a thoracoscopic approach is a large emissary venous channel in the porcine vertebral body typically located at the center of the vertebral body rostrocaudally, but inconsistently left or right of midsagittal. In live animals, this venous channel is found to bleed profusely when cut.

Intercostal spacing

Both the porcine and human midaxillary intercostal spacing gradually increased from rostral to caudal, remaining only slightly larger in humans at all levels (Table 2; significant difference only at T1–T2). The intercostal spacing was maximum at T10–T11 in both humans (mean, 15.2 mm) and swine (mean, 13.6 mm).

Disc space

For all thoracic levels combined, the mean intervertebral disc space averaged 1.6 mm at the anterior disc margin, 2.4 mm in the mid-disc, and 1.7 mm at the posterior disc margin (Table 3). The disc space was narrowest at T1–T2, remaining somewhat constant from this level down to T9–T10 before beginning to widen. The disc space was widest at T13–T14. There was no statistically significant difference between the anterior and the posterior disc space measurements ($p = 0.24$), but the disc space measured at the mid-disc was significantly greater than the anterior or posterior measurements ($p < 0.01$). All levels of the porcine spine had a significantly smaller disc space than any level of the human thoracic spine ($p < 0.0001$), which averaged 6.6 mm [4]. In the human, the disc space (noncalcified) is much less constant among levels, continuously increasing from T1–T2 to T11–T12.

Vertebral body height

The mean porcine anterior and posterior vertebral body heights (AVBH and PVBH) steadily increased from T1 to T15 (Table 4, Fig. 5). From T1 to T12, the increase in

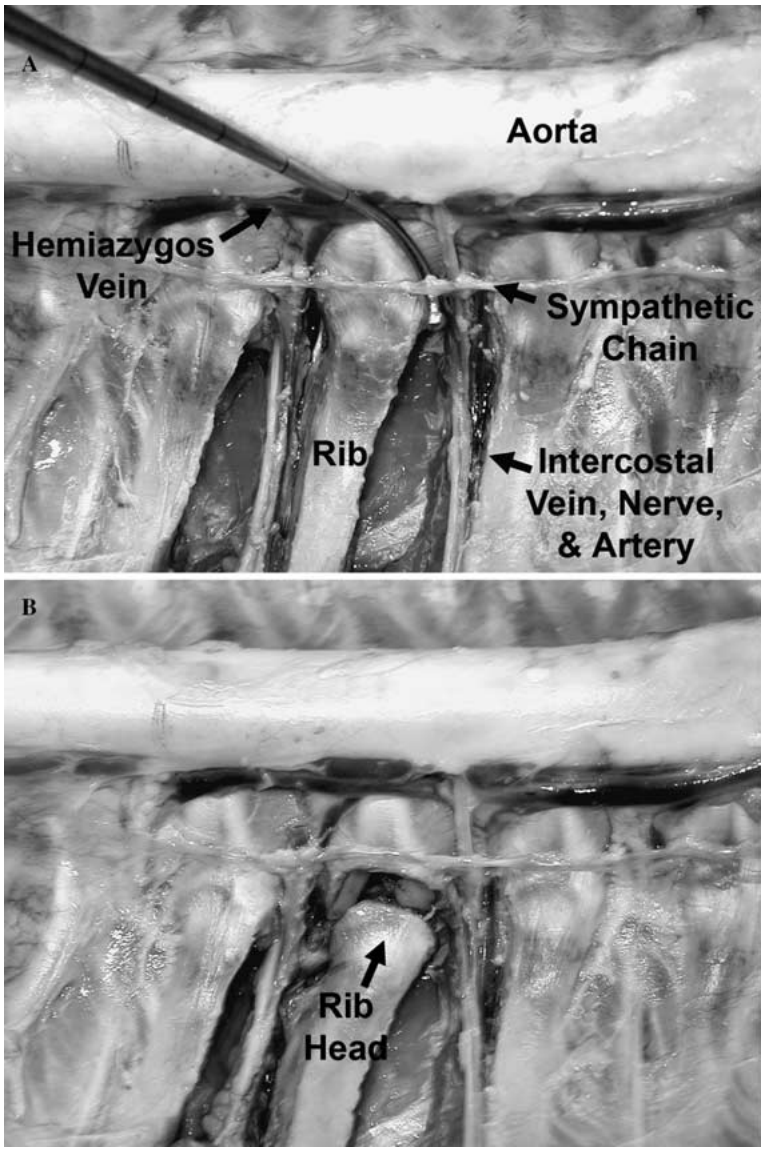

Fig. 4. Location and appearance of the sympathetic chain relative to the rib head in the left porcine thorax. **A** with the rib in position, **B** with the rib disarticulated at the costovertebral joint.

Table 2. Porcine versus human intercostal spacing (mean ± SD)

	Human	Porcine
Level	(mm)	(mm)
T1–T2	9.4 ± 1.5	8.0 ± 0.9[a]
T2–T3	10.8 ± 2.6	9.6 ± 1.9
T3–T4	10.9 ± 1.8	10.6 ± 1.4
T4–T5	11.0 ± 2.1	10.8 ± 1.2
T5–T6	12.3 ± 2.9	11.5 ± 1.1
T6–T7	12.3 ± 2.7	11.7 ± 0.9
T7–T8	13.6 ± 2.8	12.4 ± 1.0
T8–T9	14.0 ± 2.3	13.3 ± 0.8
T9–T10	13.4 ± 3.2	13.5 ± 1.3
T10–T11	15.2 ± 2.1	13.6 ± 1.3
T11–T12	12.5 ± 1.6	12.1 ± 1.5
T12–T13		11.6 ± 1.3
T13–T14		12.2 ± 1.5
T14–T15		12.2 ± 1.7

[a] Significant difference between swine and human (nonpaired two-tailed Student's *t*-test)

PVBH was 46% in the swine, as compared with 61% in the human [17]. The mean porcine AVBH and PVBH remained approximately equal at all levels, with a global mean ratio (AVBH/PVBH) of 1.02. The upper thoracic region had the most asymmetry, with AVBH 20% larger than PVBH at T1 to facilitate transition to the lordotic cervical region. The porcine PVBH often was equivalent to that of the human, although the PVBH was significantly larger in the swine than in the human at 6 of 12 levels ($p < 0.04$, Table 4).

Vertebral end plates

The mean porcine end plate width increased from T1 to T12 by a gradual 16%, as compared with the more rapid increase in end plate width in the human of 55% from T1 to T12 (Tables 5 and 6, Fig. 6a). In the swine, the end plate widths (UEW and LEW) at T12–T15 generally were significantly greater than the end plate widths at the levels rostral to T10 ($p < 0.05$). The porcine end

Table 3. Porcine versus human intervertebral disc height (mean ± SD)

	Human [4]	Porcine		
Level	Largest (mm)	Anterior (mm)	Middle (mm)	Posterior (mm)
T1–T2	4.9 ± 1.4	1.4 ± 0.3	2.1 ± 0.7	1.4 ± 0.3
T2–T3	4.9 ± 1.1	1.6 ± 0.3	2.3 ± 0.6	1.6 ± 0.4
T3–T4	5.5 ± 1.2	1.6 ± 0.3	2.3 ± 0.6	1.8 ± 0.5
T4–T5	6.0 ± 1.2	1.6 ± 0.2	2.3 ± 0.6	1.8 ± 0.4
T5–T6	6.1 ± 1.1	1.6 ± 0.3	2.1 ± 0.6	1.7 ± 0.3
T6–T7	6.3 ± 1.0	1.5 ± 0.2	1.9 ± 0.5	1.6 ± 0.3
T7–T8	6.5 ± 1.3	1.5 ± 0.2	2.1 ± 0.5	1.7 ± 0.2
T8–T9	6.7 ± 1.3	1.4 ± 0.1	2.1 ± 0.7	1.6 ± 0.2
T9–T10	7.7 ± 1.8	1.5 ± 0.2	2.3 ± 0.5	1.7 ± 0.3
T10–T11	8.5 ± 2.3	1.5 ± 0.2	2.4 ± 0.5	1.6 ± 0.3
T11–T12	9.1 ± 1.8	1.6 ± 0.3	2.6 ± 0.3	1.8 ± 0.3
T12–T13		1.7 ± 0.2	3.0 ± 0.5	1.8 ± 0.3
T13–T14		1.9 ± 0.3	3.3 ± 0.4	1.9 ± 0.3
T14–T15		1.8 ± 0.4	3.2 ± 0.5	1.7 ± 0.4

Table 4. Porcine versus human vertebral body height (mean ± SD)

	Human [17]	Porcine		
Level	PVBH (mm)	PVBH (mm)	AVBH (mm)	AVBH/PVBH (mm)
T1	14.1 ± 0.41	14.3 ± 1.08	17.1 ± 1.66	1.2 ± 0.13
T2	15.6 ± 0.58	15.5 ± 1.16	17.3 ± 1.03	1.1 ± 0.06
T3	15.7 ± 0.57	17.5 ± 0.66[a]	18.0 ± 1.20	1.0 ± 0.05
T4	16.2 ± 0.48	17.7 ± 1.01[a]	18.2 ± 1.19	1.0 ± 0.05
T5	16.2 ± 0.60	18.1 ± 1.38[a]	18.4 ± 1.42	1.0 ± 0.07
T6	17.4 ± 0.54	18.3 ± 1.24[a]	18.7 ± 0.93	1.0 ± 0.04
T7	18.2 ± 0.70	18.5 ± 1.44	19.2 ± 1.26	1.0 ± 0.07
T8	18.7 ± 0.69	19.7 ± 1.24[a]	19.1 ± 1.50	1.0 ± 0.06
T9	19.3 ± 0.59	19.9 ± 0.94	19.6 ± 1.34	1.0 ± 0.03
T10	20.2 ± 0.44	20.3 ± 1.28	20.0 ± 1.01	1.0 ± 0.03
T11	21.3 ± 0.71	20.9 ± 1.22	20.2 ± 1.39	1.0 ± 0.04
T12	22.7 ± 1.04	20.9 ± 1.06[a]	20.5 ± 1.11	1.0 ± 0.06
T13		21.1 ± 1.43	20.5 ± 1.26	1.0 ± 0.05
T14		21.4 ± 1.01	20.8 ± 1.27	1.0 ± 0.06
T15		22.3 ± 1.22	22.1 ± 1.23	1.0 ± 0.02

PVBH, posterior vertebral body height; AVBH, anterior vertebral body height
[a] Significant difference between swine and human (nonpaired two-tailed Student's *t*-test)

plate depths (UED and LED) were not significantly different among levels, increasing by only 7% from T1 to T12 (Tables 5 and 6, Fig. 6b). In contrast, the human end plate depth increased by 73% from T1 to T12. Porcine versus human UEW, LEW, UED, and LED each were significantly different at all levels ($p < 0.0001$).

The porcine thoracic end plate was more asymmetric than the human thoracic end plate. The ratio of UEW/UED averaged 1.4 in the swine, as compared with 1.1 in the human, and the ratio of LEW/LED averaged 1.5 in the swine, as compared with 1.1 in the human (Tables 5 and 6). Progressing from rostral to caudal, the porcine end plate became more kidney shaped (Fig. 2b). The porcine end plate areas increased by 25% from T1 to T12, whereas the human end plate areas increased by 195% from T1 to T12 (Tables 5 and 6). In the same human vertebra, the UEA was 71 ± 19 mm^2 (12%) smaller on the average than the LEA, whereas in the porcine vertebra, the UEA was only 9 ± 5 mm^2 (4%) smaller.

Costovertebral joints

Rostral and caudal demifacets in each vertebra allowed the costovertebral articulations to form across each disc space (Fig. 7). These joints were located at the anterosuperior and anteroinferior margins of the pedicle, except T15, which had only a superior costovertebral joint. In the human thoracic spine, the first two ribs articulate with the thoracic vertebral body of the same number. The third rib articulates with the second and third thoracic vertebral bodies and can serve as a guide to the second and third intervertebral disc spaces. This pattern continues until the 10th vertebral body. The 10th, 11th, and 12th ribs articulate with the vertebral body of the same number and are not aligned with an intervertebral disc space. In the porcine thoracic spine, the first rib was found to articulate with the last cervical vertebra and first thoracic vertebra, and this pattern continued for the remainder of the thoracic spine. Therefore, each rib

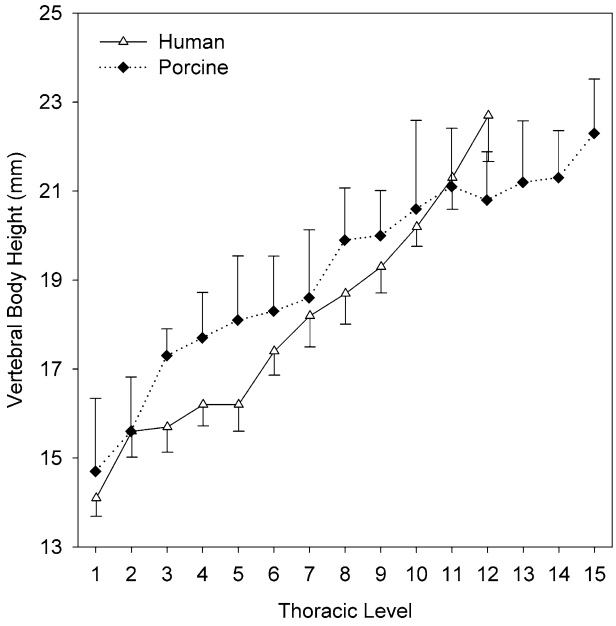

Fig. 5. Porcine versus human vertebral body height (posterior). In general, this dimension was similar in both species. Significant differences were found at T3–T8 ($p < 0.05$).

head served as a consistent guide to an intervertebral disc space in the porcine thoracic spine.

Spinal canal

The porcine spinal canal shape was triangular in the upper thoracic region and became more elliptical in the middle and lower thoracic regions (Fig. 2b). The human spinal canal shape also can be seen to vary from elliptical to more triangular among levels (Fig. 2b).

The width and depth of the porcine spinal canal decreased rapidly from T1 to T3, then remained relatively constant in the middle thoracic region (Table 7). The spinal canal depth (SCD) in the middle and lower thoracic regions was significantly smaller than at T1 and T2. From T11 to T13, the spinal canal width (SCW) increased to be significantly greater than in the middle region. In both the porcine and human thoracic spines, the SCD was similar to the SCW, with the width generally slightly larger than the depth, and ratios of SCW/SCD slightly greater than 1.0 (Table 7). The porcine SCW and SCD were significantly smaller than their human counterparts at all levels ($p < 0.0001$).

Transverse processes and foramina

Porcine thoracic transverse processes, situated at the junction of the laminae with the pedicles, were directed laterally as in the human thoracic spine. As in the human thoracic spine, porcine transverse processes articulated with a portion of the rib at a costotransverse articular joint at the anterior tip of the transverse processes from T1–T10 or T11. The transverse processes became less prominent at the lower thoracic levels than in the upper and middle thoracic spine. Progressing caudally, the costotransverse articulation gradually migrated toward the costovertebral articulation, eventually merging into one continuous articulation. In the human thoracic spine, costotransverse articulations are no longer present at level T11. In porcine specimens wherein the articulations still were visible after bone drying, the costovertebral and costotransverse articulations merged most frequently at level T11 ($n = 6$) or level T12 ($n = 3$).

Unlike the human thoracic spine, in which adjacent pedicle surfaces delineate intervertebral foramina, transverse neural foramina were found in the porcine thoracic spine that ran laterally through the centers of the pedicles (Fig. 8a). The transverse foramina communicated with the spinal canal and bifurcated to run anteroposteriorly through the transverse process at levels T1 to T10 (Fig. 8b). The lateral foramina migrated caudally and were no longer surrounded on all sides by bone after T10, instead manifesting as arched openings more like those in the human spine. At levels T11 to T14, the anteroposterior transverse process foramina remained without the lateral opening to the spinal canal. The morphology at these levels was similar to that of the human cervical transverse process foramina. The anteroposterior transverse process foramina had the largest diameters at T2, with the elliptical posterior opening averaging 5.4 ± 0.5 by 7.3 ± 0.3 mm, respectively, in the rostrocaudal and lateral diameters, as measured posteriorly. The foramen area decreased caudally to an elliptical opening at T14, averaging 5.4 ± 0.5 by 7.3 ± 0.3 mm, respectively, in the rostrocaudal and lateral diameters.

Pedicles

In the upper thoracic region, the pedicle height typically was substantially greater in the swine than in the human because the porcine pedicle houses the transverse foramen (Figs. 2 and 8). Right and left pedicle heights were significantly greater from T2 to T10 in the swine than in the human ($p < 0.05$, Table 8). The porcine pedicle height dropped off abruptly after level T10, which is the level at which the lateral transverse foramen is no longer present. At T11 and T12, because of the difference in overall vertebral size, the human pedicle heights became greater than the porcine pedicle heights. The pedicle widths generally did not vary significantly among porcine thoracic levels, although T1 had significantly wider pedicles than most other levels. Porcine and human pedicle widths were similar in many of the upper and middle thoracic regions. At level T9 and caudally, the human pedicle was wider on the average.

Facets

The facet articulations in the porcine thoracic spine were oriented similarly to those of the human in the upper thoracic region: mostly flat in the coronal plane with a slight anterior tilt and a slight outward lateral twist. At

Table 5. Porcine versus human mean (±SD) upper end plate width (UEW), depth (UED), and area (UEA)

	UEW		UED		UEW/UED		UEA	
Level	Porcine (mm)	Human [17] (mm)	Porcine (mm)	Human [17] (mm)	Porcine (mm)	Human [17] (mm)	Porcine (mm^2)	Human [17] (mm^2)
T1	18.3 ± 1.32	24.5 ± 0.85	13.4 ± 0.50	18.5 ± 0.75	1.4	1.3	193 ± 17.3	300 ± 14.3
T2	17.6 ± 1.37	24.9 ± 0.59	13.1 ± 1.24	19.6 ± 0.41	1.3	1.3	182 ± 28.2	333 ± 11.5
T3	18.0 ± 1.72	24.6 ± 0.43	13.2 ± 1.19	22.7 ± 0.75	1.4	1.1	188 ± 32.8	373 ± 16.5
T4	18.4 ± 1.45	24.5 ± 0.58	13.0 ± 1.32	23.3 ± 0.58	1.4	1.0	189 ± 32.4	381 ± 17.3
T5	19.2 ± 1.75	24.9 ± 0.77	13.5 ± 0.89	24.3 ± 0.79	1.4	1.0	204 ± 29.8	426 ± 17.9
T6	18.5 ± 1.38	26.2 ± 0.79	13.3 ± 1.15	26.0 ± 0.80	1.4	1.0	194 ± 30.1	483 ± 23.9
T7	18.6 ± 0.93	27.8 ± 0.70	13.3 ± 1.02	27.4 ± 0.54	1.4	1.0	195 ± 22.0	547 ± 25.6
T8	18.4 ± 0.95	29.5 ± 0.71	13.3 ± 0.62	27.9 ± 0.52	1.4	1.0	193 ± 17.7	605 ± 26.0
T9	19.5 ± 1.28	30.6 ± 1.06	13.8 ± 1.01	29.3 ± 1.03	1.4	1.0	212 ± 27.9	678 ± 47.0
T10	20.0 ± 1.23	31.9 ± 0.67	13.7 ± 0.86	30.5 ± 0.85	1.5	1.0	217 ± 25.5	727 ± 35.5
T11	21.0 ± 1.66	34.9 ± 0.97	13.9 ± 0.77	31.9 ± 0.71	1.5	1.1	229 ± 30.3	842 ± 41.4
T12	21.4 ± 1.90	39.0 ± 0.58	14.2 ± 0.92	32.8 ± 1.21	1.5	1.2	240 ± 35.3	954 ± 44.0
T13	22.4 ± 1.72		14.2 ± 1.20		1.6		252 ± 38.1	
T14	23.0 ± 1.48		14.9 ± 1.20		1.5		270 ± 37.1	
T15	24.6 ± 0.56		15.3 ± 0.64		1.6		296 ± 14.8	

Table 6. Porcine compared to human mean (±SD) lower end plate width (LEW), depth (LED), and area (LEA)

	LEW		LED		LEW/LED		LEA	
Level	Porcine (mm)	Human [17] (mm)	Porcine (mm)	Human [17] (mm)	Porcine (mm)	Human [17] (mm)	Porcine (mm^2)	Human [17] (mm^2)
T1	19.4 ± 2.86	27.8 ± 0.64	13.2 ± 1.10	19.7 ± 0.52	1.5	1.4	202 ± 45.2	376 ± 14.5
T2	18.8 ± 1.43	27.4 ± 0.65	13.2 ± 0.83	21.6 ± 0.64	1.4	1.3	194 ± 19.7	398 ± 10.9
T3	18.4 ± 0.85	25.9 ± 0.87	13.4 ± 1.54	23.3 ± 0.75	1.4	1.1	195 ± 29.1	412 ± 18.1
T4	18.5 ± 1.27	26.0 ± 0.92	13.4 ± 1.09	24.5 ± 0.78	1.4	1.1	196 ± 28.2	444 ± 20.8
T5	18.8 ± 1.11	27.0 ± 0.96	13.4 ± 1.06	25.8 ± 0.77	1.4	1.0	198 ± 23.3	495 ± 24.5
T6	19.1 ± 1.25	28.2 ± 0.82	13.7 ± 0.86	26.9 ± 0.67	1.4	1.0	205 ± 22.3	552 ± 21.1
T7	19.1 ± 0.85	29.1 ± 0.69	13.7 ± 0.99	28.5 ± 0.87	1.4	1.0	206 ± 22.0	603 ± 24.5
T8	19.4 ± 0.94	30.5 ± 0.70	13.5 ± 0.94	29.4 ± 0.71	1.4	1.0	206 ± 20.5	664 ± 28.6
T9	20.4 ± 1.64	33.0 ± 1.10	13.9 ± 1.23	31.0 ± 0.89	1.5	1.1	225 ± 36.2	755 ± 44.5
T10	21.1 ± 1.32	35.4 ± 0.98	13.7 ± 1.16	31.6 ± 1.11	1.5	1.1	227 ± 32.2	834 ± 43.2
T11	22.0 ± 1.68	39.1 ± 0.71	14.0 ± 1.07	31.8 ± 0.78	1.6	1.2	243 ± 32.7	945 ± 44.3
T12	22.5 ± 1.56	42.1 ± 0.91	14.3 ± 0.80	33.4 ± 0.78	1.6	1.3	253 ± 29.0	1024 ± 49.8
T13	23.4 ± 1.67		14.4 ± 1.07		1.6		266 ± 35.4	
T14	24.0 ± 1.34		14.5 ± 1.32		1.7		273 ± 34.7	
T15	25.3 ± 0.71		15.1 ± 1.35		1.7		301 ± 26.0	

the human thoracolumbar junction (T12–L1), the morphology abruptly shifts such that the superior facet articulation of L1 laterally encompasses the inferior facet articulation of T12, with the facet surfaces sharply twisting inward laterally and shifting from a coronal plane orientation to a sagittal plane orientation. This transition occurs in the porcine thoracic spine well before the lumbar region, with articulations of this shape appearing first at level T9–T10 or T10–T11. The difference in facet orientation can be seen from an axial perspective (Fig. 2b).

Discussion

Positioning and portal placement

Because the general shape of the swine's back prevents a true supine orientation, the preferred surgical position is the left lateral decubitus position with the right side up. This position is commonly used for thoracoscopic surgery in human patients [1, 6]. In a left-sided approach, mobilization of the aortic arch and hemiazygos vein is necessary. However, this procedure has been reported without any complication [15]. The absence of the azygos vein on the right side is a notable difference from that of human patients in the lateral decubitus position. It is important to instruct students concerning the absence of this prominent structure to avoid confusion in using the porcine model for teaching.

For general purpose teaching, the best working area is between T6 and T10. The attachment of the longus colli restricts an anterolateral approach rostrally through T5. In the same way, the psoas muscle and the diaphragm limit the ability to access levels T13 and caudally. Wall et al. [22] also stated that the anatomy of T8 and T9 more closely resembles that of the midthoracic human spine than that of other levels. Finally, the transition from a human thoracic-like to a

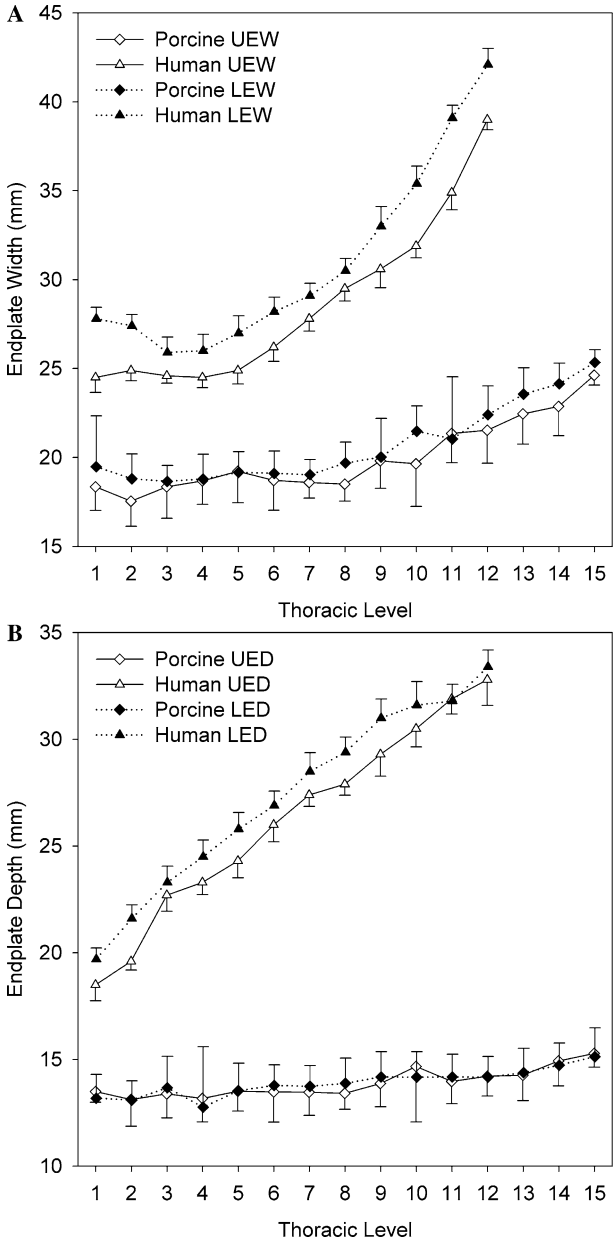

Fig. 6. Porcine versus human vertebral end plate widths (**A**) and depths (**B**). Both dimensions remain relatively constant throughout the porcine thoracic spine, whereas they increase steadily in the human thoracic spine. Within the same vertebra in the porcine thoracic spine, the upper and lower end plate widths and depths are almost identical, whereas in the human thoracic spine, the lower end plate has substantially larger dimensions than the upper end plate.

human lumbar-like facet orientation was found to occur most often in swine at T10–T11.

The points of portal entries should be selected according to the level of surgery and the procedure being performed. A good reference in the swine is palpation of the xiphoid process, which always was aligned with the sixth intercostal space and the T5–T6 disc. Under fluoroscopy, the spinous processes are readily apparent, and the approximate level can be estimated on the basis of the distinctive tapering in spinous process length from upper to lower thoracic regions (Fig. 2a). A dried porcine spinal column with numbered spinous processes should be available for such references.

To achieve the optimal angle of endoscopic tools, the portal for the endoscope is best positioned between the posterior and middle axillary lines, and the working portals are best positioned in the midaxillary line or between the middle and anterior axillary lines. If an extensive multilevel approach is needed for instrumentation, multiple portals can be placed in the middle axillary line, and the endoscope can be repositioned in different portals during the procedure [3, 8].

At T3–T4 and below, the mean porcine intercostal spacing was found to be 10.6 to 13.6 mm, as compared with the mean human intercostal spacing of 10.9 to 15.2 mm. Therefore, in both the porcine model and human patients, the appropriate diameter of the portals commonly is 10 mm or less. Alternatively, Dickman and Fessler [7] recommended using rigid thoracoports of 12 mm, which can be forced in place although oversized rather than flexible portals. To achieve better scope and tool mobility, the portals can be cut to custom length.

Because the porcine chest is narrow, the distance from the portal to the thoracic column is closer than in the human. Therefore, the endoscope tends to be positioned too close to the spine, with the result that an abnormally magnified perspective appears. Special care must be taken to maintain an appropriate distance from the spinal column. The tip of the endoscope should be positioned superficially, immediately inside the thorax.

Sympathectomy

The porcine sympathetic chain is located adjacent to the rib heads (Fig. 4). This positioning is similar to the location in the human spine, so sympathectomy in the porcine model is very much analogous to the procedure in humans. Consideration should be given to the locations of the hemiazygos and intercostal veins, and it should be realized that the azygos vein is absent in swine on the right side, but present in the human, and should be respected during sympathectomy.

Discectomy

In swine, an easy marker for each disc level is the rib. However, it should be remembered that the ribs are not aligned with the disc at all thoracic levels in the human. It has been documented that discectomy in the porcine model is far more challenging than in the human because of narrow disc space and small thoracic volume [13]. Because of the narrow porcine disc height, end plate and partial vertebral body resection via drilling and curettage may be helpful to allow room for the insertion of tools and for better visualization of the thecal sac [3, 13].

Corpectomy

In swine, the vertebral bodies are more cylindrical in shape than in the human, where they are elongated

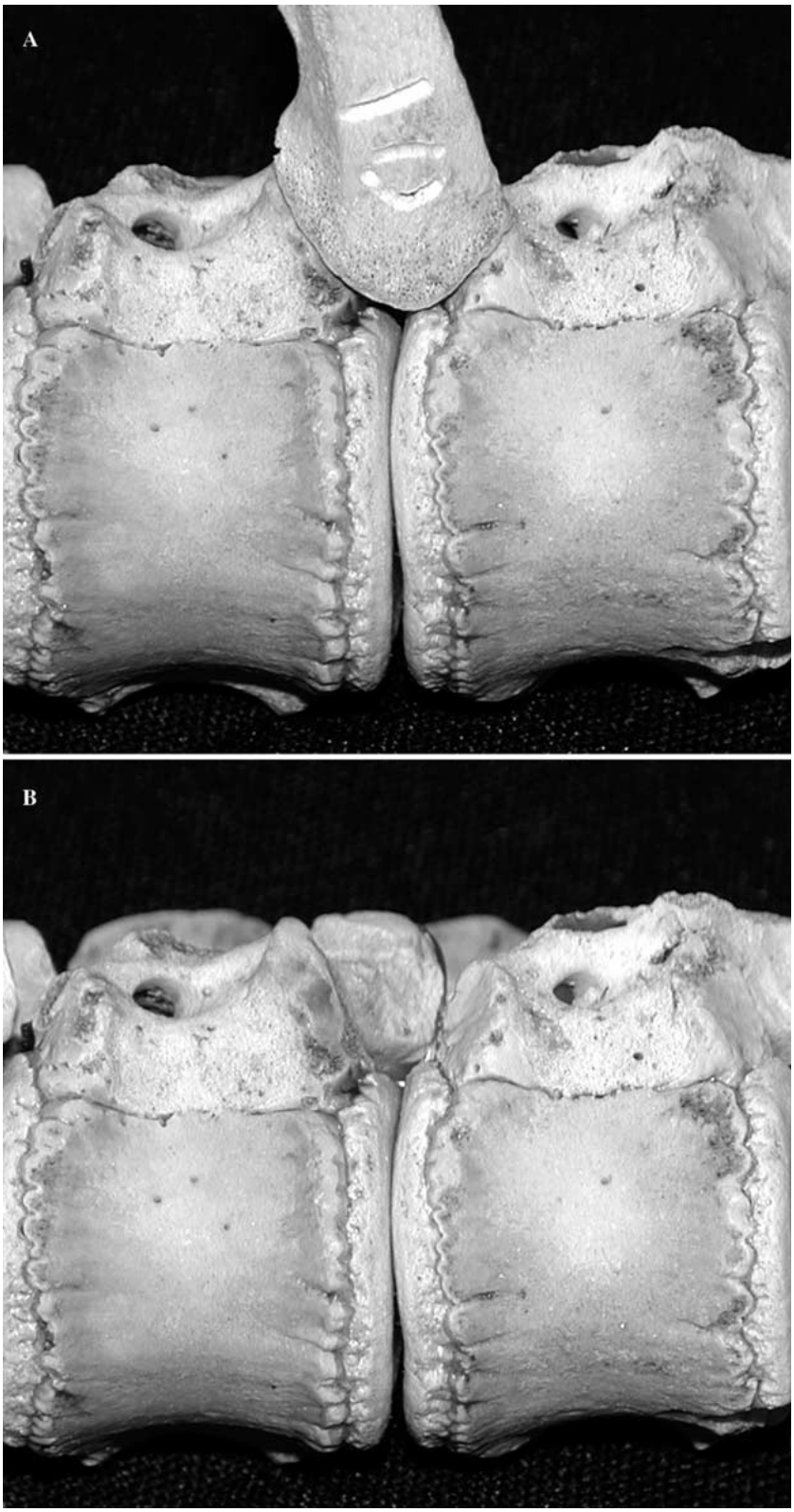

Fig. 7. Dried right anterolateral porcine thoracic vertebrae demonstrating the appearance and location of the porcine costovertebral joint. This joint is consistently located at the level of the intervertebral disc. **A** rib in place. **B** rib removed.

anteroposteriorly (Fig. 2B). Therefore, in drilling during corpectomy, the spinal canal will be reached more quickly in the porcine model than during actual surgery in humans. In addition, bleeding from the emissary vein in the vertebral body will need to be controlled using bipolar coagulation and hemostatic agents.

Table 7. Porcine versus human mean (±SD) spinal canal width (SCW) and depth (SCD)

	SCW		SCD		SCW/SCD	
	Porcine (mm)	Human [17] (mm)	Porcine (mm)	Human [17] (mm)	Porcine (mm)	Human [17] (mm)
T1	14.7 ± 0.66	21.8 ± 0.71	13.6 ± 1.68	16.4 ± 0.42	1.1	1.3
T2	12.7 ± 1.36	19.5 ± 0.34	11.9 ± 1.39	15.3 ± 1.25	1.1	1.3
T3	11.4 ± 0.80	18.3 ± 0.54	10.6 ± 0.49	15.9 ± 1.09	1.1	1.2
T4	11.2 ± 0.73	17.0 ± 0.57	10.5 ± 0.58	16.2 ± 0.89	1.1	1.0
T5	11.0 ± 1.02	17.1 ± 0.68	10.1 ± 0.94	16.3 ± 0.72	1.1	1.0
T6	11.7 ± 2.27	17.3 ± 0.74	10.6 ± 1.20	16.5 ± 0.62	1.1	1.0
T7	10.9 ± 0.78	17.3 ± 0.83	10.2 ± 1.08	16.1 ± 0.69	1.1	1.1
T8	11.5 ± 1.09	17.7 ± 0.63	9.3 ± 1.15	15.9 ± 0.76	1.2	1.1
T9	12.1 ± 1.14	17.9 ± 1.19	8.9 ± 1.00	15.7 ± 0.82	1.4	1.1
T10	12.4 ± 1.17	18.2 ± 0.78	8.9 ± 0.98	15.5 ± 0.70	1.4	1.2
T11	12.9 ± 1.09	19.4 ± 0.95	9.6 ± 1.19	16.0 ± 0.46	1.3	1.2
T12	13.3 ± 1.28	22.2 ± 1.12	9.7 ± 0.98	18.1 ± 0.62	1.4	1.2
T13	13.5 ± 1.25		9.5 ± 1.09		1.4	
T14	13.3 ± 1.05		9.3 ± 0.87		1.4	
T15	12.8 ± 0.73		9.4 ± 1.38		1.4	

Spinal canal access

Past research has shown that porcine spinal canal visualization is difficult to achieve and not recommended [5, 13, 15]. Porcine thoracic pedicles have greater height than human pedicles because they house a neural foramen. It is difficult and time consuming to unroof the nerve root that passes through this foramen, and it is not analogous to the anatomy around the nerve root in the human spine. It is therefore better not to spend excessive time attempting to remove the porcine pedicle. Instead, the dura should be identified by locating the nerve root and foramen with a probe. The vertebral body then can be resected along the dural margin to reach the spinal canal.

If pedicle resection is desired, the rib head should be removed first. Intercostal fat tissue should be identifiable before the segmental vessels are reached. In resecting the pedicle, it is important that the height of the porcine pedicle is greater than in the human above T11. However, the width of the pedicle can be the same or more narrow than in the human. During resection of the pedicle, there should be bleeding. The source of the bleeding is the segmental artery, which can be controlled by bipolar coagulation and hemostatic agents.

Facet access

The anatomy differences between human and porcine facets, particularly the transition in geometry to a human lumbar-like geometry before the last thoracic level, may be a result of load-bearing differences because swine are quadrupedal, whereas humans are bipedal [20]. Whatever the cause, it should be recognized that a facet orientation similar to the thoracic facet orientation in humans occurs in swine only rostrally to the T10–T11 (occasionally the T9–T10) facet joints. Therefore, in the attempt to access the facet joints thoracoscopically, joints caudal to the transition level will be blocked by a layer of bone from the inferior facet as they would be in the human lumbar spine.

Instrumentation

Spinal instrumentation via thoracoscopy has been reported in the literature [3, 8, 12]. The main consideration during instrumentation using a porcine model is the difference in vertebral body dimensions. The vertebral body width and height are similar between swine and humans, but the vertebral body depth is substantially less in swine. Because of the more cylindrical shape, anterolateral plates would tend to lie facing less laterally in the porcine model, forcing the screw trajectories to be more anteroposteriorly oriented. Consequently, screws inserted anterolaterally in the vertebral body are likely to reach the spinal canal sooner in the porcine model than in humans. Therefore, anterolateral screw length probably should not exceed 15 mm in the porcine model, and interbody cage depth probably should not exceed 10 mm.

Additional uses of a porcine model

Instead of using the porcine model strictly for teaching purposes, some authors have described the use of a porcine model to test the feasibility of complex endoscopic approaches [2, 19]. Rubino et al. [19] used a 30° angle endoscope to view the upper thoracic and cervical spine with an entrance portal at the anterior border of the sternocleidomastoid muscle. These authors reported excellent visualization of the entire cervical spine. Burgos et al. [2] used swine to test the feasibility of a method for exposing the thoracolumbar spine. Before attempting the procedure in patients, these authors determined that in swine, the most effective method for exposure was an initial standard thoracoscopic approach followed by a retroperitoneal endoscopic approach. As with the use of the porcine model in teaching, it is crucial to understand differences between the porcine and human anatomies to draw valid conclusions from such studies.

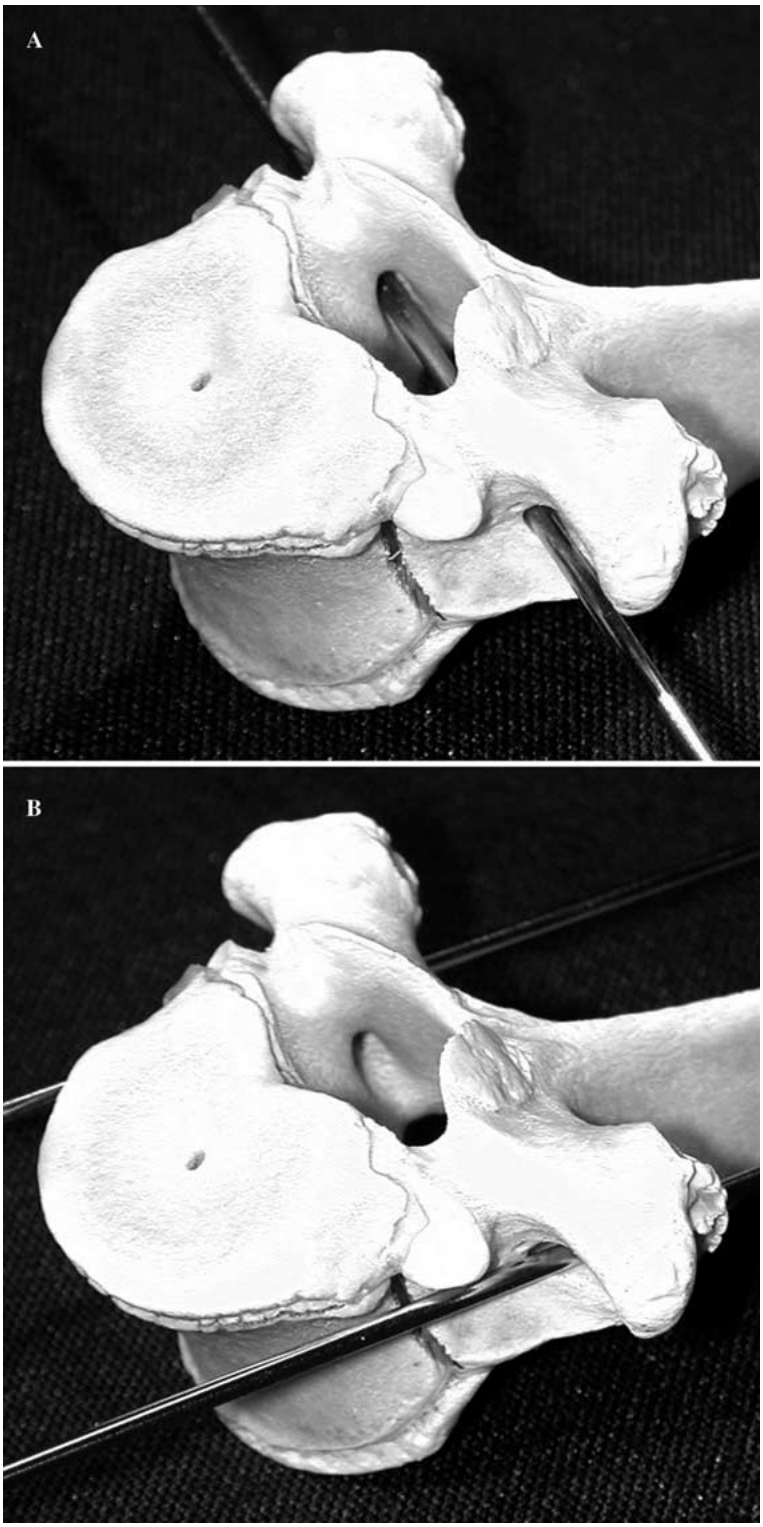

Fig. 8. Appearance and location of the porcine transverse foramina. **A** lateral foramina. **B** anteroposterior foramina. In each view, 1.5-mm stainless steel guidewires have been placed through the foramina to demonstrate their continuity and orientation.

Study limitations

In this study, the quantitative anatomy of the laminae, spinous processes, and facets was not included because thoracoscopy provides no access to these posterior spinal elements. Assumptions were made such as the elliptical cross-sectional area of the spinal canal.

In addition to anatomic differences, another consideration regarding the use of a porcine model in thoracoscopy is the difference in bone quality. Typically, porcine bone is substantially harder than human bone. Also, because the study animals were immature, some structures such as the end plates were not fully fused, creating differences in the response of these regions

Table 8. Porcine versus human mean (±SD) right pedicle width (RPW) and height (RPH) and left pedicle width (LPW) and height (LPH)

Level	RPW		LPW		RPH		LPH		RPH/RPW		LPH/LPW	
	Porcine (mm)	Human [17] (mm)	Porcine (mm)	Human [17] (mm)	Porcine (mm)	Human [17] (mm)	Porcine (mm)	Human [17] (mm)	Porcine (mm)	Human [17] (mm)	Porcine (mm)	Human [17] (mm)
T1	9.2 ± 1.74	8.2 ± 0.44	10.4 ± 1.70[a]	8.7 ± 0.53	10.8 ± 2.11[a]	9.3 ± 0.53	10.4 ± 2.06	9.9 ± 0.41	1.2	1.1	1.0	1.1
T2	7.2 ± 0.77[a]	8.4 ± 1.06	7.7 ± 0.98	7.9 ± 0.97	12.8 ± 0.91[a]	11.1 ± 0.44	13.2 ± 1.38[a]	11.6 ± 0.30	1.8	1.3	1.7	1.5
T3	6.8 ± 1.35	7.0 ± 0.78	6.9 ± 1.19	6.5 ± 0.55	14.1 ± 1.04[a]	11.8 ± 0.23	13.8 ± 0.96[a]	12.0 ± 0.32	2.1	1.7	2.0	1.4
T4	6.9 ± 0.95[a]	5.5 ± 0.71	6.9 ± 1.37	7.0 ± 0.49	14.1 ± 0.99[a]	11.9 ± 0.46	14.3 ± 1.17[a]	12.2 ± 0.50	2.1	2.2	2.1	1.4
T5	6.7 ± 0.82	6.2 ± 0.53	6.7 ± 0.93[a]	5.7 ± 0.38	14.1 ± 0.98[a]	11.2 ± 0.51	14.0 ± 0.93[a]	11.4 ± 0.36	2.1	1.8	2.1	2.0
T6	6.3 ± 1.23	6.0 ± 0.78	7.1 ± 0.75[a]	6.0 ± 0.87	14.5 ± 1.34[a]	12.0 ± 0.44	14.9 ± 1.00[a]	11.6 ± 0.47	2.3	2.0	2.1	1.9
T7	7.2 ± 0.83	6.5 ± 0.80	7.2 ± 0.39[a]	5.2 ± 0.45	15.2 ± 1.44[a]	11.8 ± 0.30	15.4 ± 1.10[a]	12.2 ± 0.27	2.1	1.8	2.1	2.3
T8	6.9 ± 0.86	6.7 ± 0.35	6.7 ± 0.64	6.7 ± 0.63	15.7 ± 1.19[a]	12.5 ± 0.52	15.9 ± 1.19[a]	12.5 ± 0.41	2.3	1.9	2.4	1.9
T9	6.8 ± 1.11[a]	7.6 ± 0.54	7.6 ± 0.82	7.7 ± 0.65	15.6 ± 1.25[a]	13.9 ± 0.79	15.8 ± 1.31[a]	13.8 ± 0.55	2.3	1.8	2.1	1.8
T10	6.5 ± 1.36[a]	8.3 ± 0.70	7.6 ± 1.27[a]	9.7 ± 0.78	15.5 ± 1.07[a]	14.7 ± 0.49	15.8 ± 1.20[a]	15.0 ± 0.24	2.4	1.8	2.1	1.6
T11	7.1 ± 0.97[a]	8.8 ± 0.43	7.0 ± 1.33[a]	10.7 ± 0.84	16.7 ± 1.40	16.9 ± 0.49	16.1 ± 0.95[a]	17.8 ± 0.29	2.4	1.9	2.3	1.7
T12	7.6 ± 0.82[a]	8.8 ± 0.81	7.3 ± 0.88[a]	8.6 ± 0.68	16.1 ± 1.69	16.5 ± 0.71	16.4 ± 0.99	16.8 ± 0.94	2.1	1.9	2.3	1.9
T13	7.6 ± 0.66		6.9 ± 0.84		16.4 ± 1.39		17.0 ± 2.34		2.2		2.5	
T14	8.1 ± 1.25		7.6 ± 1.10		17.9 ± 1.22		17.7 ± 1.94		2.2		2.3	
T15	8.6 ± 0.62		8.2 ± 1.29		19.0 ± 1.12		19.6 ± 2.23		2.2		2.4	

[a] Significant difference between swine and human ($p < 0.05$, nonpaired two-tailed Student's *t*-test)

under drilling or curettage. Mechanical differences were not investigated in this study.

Conclusion

The results of this study provide quantitative and qualitative anatomic documentation of differences between human and porcine thoracic spines. This information should enable surgeons using swine in learning thoracoscopic techniques to understand better how the porcine model differs from what will be encountered during actual surgery. With regard to general teaching of thoracoscopy, a right-sided thoracoscopy between T6 and T10 probably is most similar to that in the human anatomically and least hindered by muscle attachments

Acknowledgments. The authors thank Luis Perez, MD, Geun Sung Song, MD, and Mary Fifield, BSE for their assistance with this study.

References

1. Arlet V (2000) Anterior thoracoscopic spine release in deformity surgery: a meta-analysis and review. Eur Spine J 9(Suppl 1): S17–S23
2. Burgos J, Rapariz JM, Gonzalez-Herranz P (1998) Anterior endoscopic approach to the thoracolumbar spine. Spine 23: 2427–2431
3. Caputy A, Starr J, Riedel C (1995) Video-assisted endoscopic spinal surgery: thoracoscopic discectomy. Acta Neurochir (Wien) 134: 196–199
4. Chanchairujira K, Chung CB, Kim JY, Papakonstantinou O, Lee MH, Clopton P, Resnick D (2004) Intervertebral disk calcification of the spine in an elderly population: radiographic prevalence, location, and distribution and correlation with spinal degeneration. Radiology 230: 499–503
5. Connolly PJ, Ordway NR, Sacks T, Kolata R, Yuan HA (1999) Video-assisted thoracic diskectomy and anterior release: a biomechanical analysis of an endoscopic technique. Orthopedics 22: 923–926
6. Dickman CA, Detwiler PW, Porter RW (2000) Endoscopic spine surgery. Clin Neurosurg 46: 526–553
7. Dickman CA, Fessler RG (1999) Education and credentialing for thoracoscopic spine surgery. In: Dickman CA, Rosenthal DJ, Perin NI (eds). Thoracoscopic spine surgery. Thieme, New York, pp 19–26
8. Ebara S, Kamimura M, Itoh H, Kinoshita T, Takahashi J, Takaoka K, Ohtsuka K (2000) A new system for the anterior restoration and fixation of thoracic spinal deformities using an endoscopic approach. Spine 25: 876–883
9. Han PP, Dickman CA (2002) Thoracoscopic resection of thoracic neurogenic tumors. J Neurosurg Spine 96: 304–308
10. Han PP, Gottfried ON, Kenny KJ, Dickman CA (2002) Biportal thoracoscopic sympathectomy: surgical techniques and clinical results for the treatment of hyperhidrosis. Neurosurgery 50: 306–311
11. Han PP, Kenny K, Dickman CA (2002) Thoracoscopic approaches to the thoracic spine: experience with 241 surgical procedures. Neurosurgery 51: S88–S95
12. Horn EM, Henn JS, Lemole GM Jr, Hott JS, Dickman CA (2004) Thoracoscopic placement of dual-rod instrumentation in thoracic spinal trauma. Neurosurgery 54: 1150–1153
13. Horowitz MB, Moossy JJ, Julian T, Ferson PF, Huneke K (1994) Thoracic discectomy using video-assisted thoracoscopy. Spine 19: 1082–1086
14. Karahalios DG, Apostolides PJ, Vishteh AG, Dickman CA (1997) Thoracoscopic spinal surgery: treatment of thoracic instability. Neurosurg Clin North Am 8: 555–573
15. Muhlbauer M, Ferguson J, Losert U, Koos WT (1998) Experimental laparoscopic and thoracoscopic discectomy and instru-

mented spinal fusion: a feasibility study using a porcine model. Minim Invasive Neurosurg 41: 1–4
16. Olinger A, Pistorius G, Lindemann W, Vollmar B, Hildebrandt U, Menger MD (1999) Effectiveness of a hands-on training course for laparoscopic spine surgery in a porcine model. Surg Endosc 13: 118–122
17. Panjabi MM, Takata K, Goel V, Federico D, Oxland T, Duranceau J, Krag M (1991) Thoracic human vertebrae: quantitative three-dimensional anatomy. Spine 16: 888–901
18. Rosenthal D, Dickman CA (1998) Thoracoscopic microsurgical excision of herniated thoracic discs. J Neurosurg 89: 224–235
19. Rubino F, Deutsch H, Pamoukian V, Zhu JF, King WA, Gagner M (2000) Minimally invasive spine surgery: an animal model for endoscopic approach to the anterior cervical and upper thoracic spine. J Laparoendosc Adv Surg Tech A 10: 309–313
20. Smit TH (2002) The use of a quadruped as an in vivo model for the study of the spine: biomechanical considerations. Eur Spine J 11: 137–144
21. Visocchi M, Masferrer R, Sonntag VK, Dickman CA (1998) Thoracoscopic approaches to the thoracic spine. Acta Neurochir (Wien) 140: 737–743
22. Wall EJ, Bylski-Austrow DI, Shelton FS, Crawford AH, Kolata RJ, Baum DS (1998) Endoscopic discectomy increases thoracic spine flexibility as effectively as open discectomy: a mechanical study in a porcine model. Spine 23: 9–15